Applied Physics B (2018) 124:31
https://doi.org/10.1007/s00340-018-6896-y

Applied Physics B
Lasers and Optics

520-μJ mid-infrared femtosecond laser at 2.8 μm by 1-kHz KTA optical parametric amplifier

Huijun He[1,2] · Zhaohua Wang[1] · Chenyang Hu[1,2] · Jianwang Jiang[3] · Shuang Qin[1] · Peng He[3] · Ninghua Zhang[3] · Peilong Yang[3] · Zhiyuan Li[4] · Zhiyi Wei[1,2]

Received: 5 December 2017 / Accepted: 12 January 2018 / Published online: 31 January 2018

Abstract
We report on a 520-μJ, 1-kHz mid-infrared femtosecond optical parametric amplifier system driven by a Ti:sapphire laser system. The seeding signal was generated from white-light continuum in YAG plate and then amplified in four non-collinear amplification stages and the idler was obtained in the last stage with central wavelength at 2.8 μm and bandwidth of 525 nm. To maximize the bandwidth of the idler, a theoretical method was developed to give an optimum non-collinear angle and estimate the conversion efficiency and output spectrum. As an experimental result, laser pulse energy up to 1.8 mJ for signal wave and 520 μJ for idler wave were obtained in the last stage under 10-mJ pump energy, corresponding to a pump-to-idler conversion efficiency of 5.2%, which meets well with the numerical calculation.

Mid-infrared femtosecond laser science and technology meet great opportunities with wide application in high-resolution spectroscopy, biomedical science, strong-field physics, etc. In high-order harmonic generation (HHG) process, the ponderomotive energy of oscillating free electron $U_p \propto \lambda^2$, implying that HHG with higher cut-off energy can be realized by wavelength scaling of pump source [1, 2]. However, some numerical and experimental studies on laser wavelength scaling find that the high harmonic yield falls with $\lambda^{-6.5}$ [3]. Much higher photon flux is needed for mid-infrared laser than common Ti:sapphire lasers when working as HHG pump source and high-energy mid-infrared few-cycle laser working at high repetition rate is thus in demand.

Mid-infrared few-cycle lasers are mainly accomplished by optical parametric amplification (OPA) or optical parametric chirped pulse amplification (OPCPA). Millijoule-level, kHz lasers with central wavelength around 2 μm have been established in several research groups [4–6]. Based on this kind of laser source, soft X-ray is generated [7, 8] and attosecond pulse as short as 53 as is realized recently [9, 10]. 10-mJ-level mid-infrared laser systems centered at 3.9 μm and tunable from 3.3 to 3.95 μm both with pulse duration around 100 fs are performed [11, 12], driven by the former source 1.6-keV tabletop X-ray generation was realized [13]. Up to now, the repetition rate of millijoule-level femtosecond lasers around 3 μm is mainly in the range of 10–20 Hz, under which either characterization of attosecond pulses or experiment like time-resolved spectroscopy is not viable. For longer wavelength lasers, several attempts have been made to realize femtosecond pulse output at 5 μm wavelength range [14, 15], and most recently, L. Grafenstein et al. realized 1.3 mJ output at 1 kHz with wavelength centered at 5.1 μm and the pulses were recompressed to 75 fs [16]. Whereas such systems usually need pump source working at 2 μm which is not easy to get, there is few group which can perform such a kind of experiments. To get intense broadband mid-infrared pulses at comparatively high repetition rate, we developed a mid-infrared femtosecond OPA system driven by commonly used Ti:sapphire amplifier. Theoretical

This article is part of the topical collection "Mid-infrared and THz Laser Sources and Applications" guest edited by Wei Ren, Paolo De Natale and Gerard Wysocki.

✉ Zhaohua Wang
zhwang@iphy.ac.cn

✉ Zhiyi Wei
zywei@iphy.ac.cn

[1] Beijing National Laboratory for Condensed Matter Physics, Institute of Physics, Chinese Academy of Sciences, Beijing 100190, China

[2] University of Chinese Academy of Sciences, Beijing 100049, China

[3] School of Physics and Optoelectronics Engineering, Xidian University, Xi'an 710071, China

[4] College of Physics and Optoelectronics, South China University of Technology, Guangzhou 510640, China

method was developed to give an optimum non-collinear angle between pump and signal.

Our system layout is illustrated in Fig. 1. A home-made Ti:sapphire laser acts as pump source which delivers 40-fs pulses at 1 kHz with energy up to 20 mJ. Due to the limitation of continuum generation inside the non-collinear crystal in the last stage, only 12 mJ of the pump pulse energy is used in our experiment. About 85% of pump energy was sent into the final stage using a beam splitter. About 2-mJ pump energy was applied to generate signal pulse and preamplify it. A small portion of the pump was focused onto a 3-mm YAG plate to generate white-light continuum (WLC). Neutral density filters and an iris were placed in front of the focusing lens to maintain single filament generation. The WLC was initially amplified in a 1-mm BBO (Type I, $\theta = 28.5°$) which is pumped by the second harmonic of part of the Ti:sapphire laser output. The pump and the signal were both loosely focused onto the BBO. Due to the dispersion induced by lenses and the YAG plate, the WLC was stretched to longer pulse duration than the pump wave. By adjusting time delay between the signal and the pump, some part of the WLC was selected for subsequent amplification. Up to 1.3 μJ of the signal energy was reached during the first-stage amplification.

The successive three stages of parametric amplification were conducted in non-collinear configuration to realize broadband output. KTA crystal was chosen as parametric gain medium which has a large transparency ranging from 350 to 4000 nm, high nonlinearity and high damage threshold and has been widely used in parametric generation and amplification of mid-infrared pulses [17, 18]. All KTA crystals in the three stages are 3-mm thick (Type II, $\theta = 40°$, $\varphi = 90°$).

The dispersion characteristics of the KTA crystal can be modified by introducing a non-collinear angle, which strongly affects output parametric bandwidth. Phase-matching conditions under different configurations of collinear amplification and non-collinear amplification with non-collinear angle of 3°, 4°, and 5°, respectively, are shown in Fig. 2. The color bar indicates phase-matching efficiency determined by $\mathrm{sinc}^2(\Delta kL/2)$, where Δk represents phase mismatch and L is the length of KTA crystal. The bright yellow region corresponds to the area with high phase-matching efficiency in frequency domain. The solid color lines indicate different idler wavelengths. In femtosecond OPA process, both conditions of broadband signal amplification and broadband idler generation are reached simultaneously. Thus, this simulation can be a guide for both broadband signal amplification design and difference-frequency generation (DFG) design. The broader bright region, the more components of the pump, and signal are involved in the OPA process and the more idler components cross through the bright region, which means that broader bandwidth is generated for idler in the last DFG stage. With this method, we can preestimate an approximate angle we need. In our experiment, the pumping beam has a spectral span of 787–817 nm (full-width at half-maximum). The non-collinear angle of 4° was chosen to make full use of the pump components.

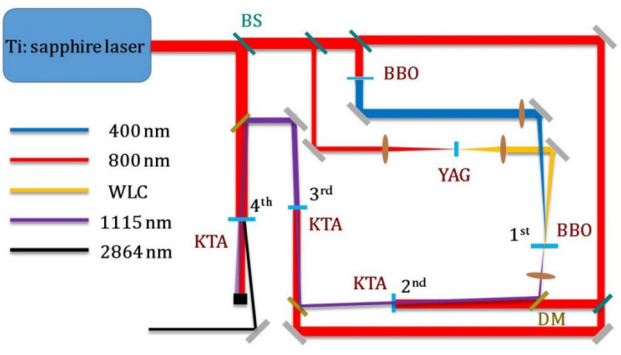

Fig. 1 Schematic layout of the 2.8-μm laser system. *BS* beam splitter; *DM* dichroic mirror. *WLC* white-light continuum. Different wavelengths are marked with different colors annotated on the left side

To interpret the impact of different configurations on phase-matching condition, we developed a theoretical method to further illustrate the non-collinear phase-matching process and evaluate the output bandwidth by solving a series of coupled wave equations in frequency domain simultaneously. First, we split the spectrum of the pump, signal, and idler waves into discrete parts by means of discrete Fourier transform. Then, we reconsidered the second-order nonlinear polarization. For each individual frequency component, the corresponding nonlinear polarization is involved in a series of terms under the law of energy conservation, which indicates mutual coupled nonlinear interactions. Assuming all series of mixing waves are plane waves, Eqs. (1)–(3) are derived from Maxwell equations under the slowly varying envelope approximation. The contribution of each nonlinear process is determined by the corresponding phase-matching condition and the amplitude of the corresponding electric field:

$$\frac{\mathrm{d}E^{\mathrm{pump}}_{\mathrm{eff},o}(\omega_o)}{\mathrm{d}z} = \frac{i\omega_o}{n^o_{\omega_o}(\theta_{\mathrm{pump}})c} d_{eff} \sum_{p=1}^{N_2}\sum_{q=1}^{N_3} E^{\mathrm{sig}}_{\mathrm{eff},p}(\omega_p) E^{\mathrm{idler}}_{\mathrm{eff},q}(\omega_q) \mathrm{e}^{-i\Delta kz} \delta_{\omega_o,\omega_p+\omega_q}, \tag{1}$$

$$\frac{\mathrm{d}E^{\mathrm{sig}}_{\mathrm{eff},p}(\omega_p)}{\mathrm{d}z} = \frac{i\omega_p}{n^e_{\omega_p}(\theta_{\mathrm{sig}})c} d_{\mathrm{eff}} \sum_{o=1}^{N_1}\sum_{q=1}^{N_3} E^{\mathrm{pump}}_{\mathrm{eff},o}(\omega_o) \left[E^{\mathrm{idler}}_{\mathrm{eff},q}(\omega_q)\right]^* e^{i\Delta kz} \delta_{\omega_o,\omega_p+\omega_q}, \tag{2}$$

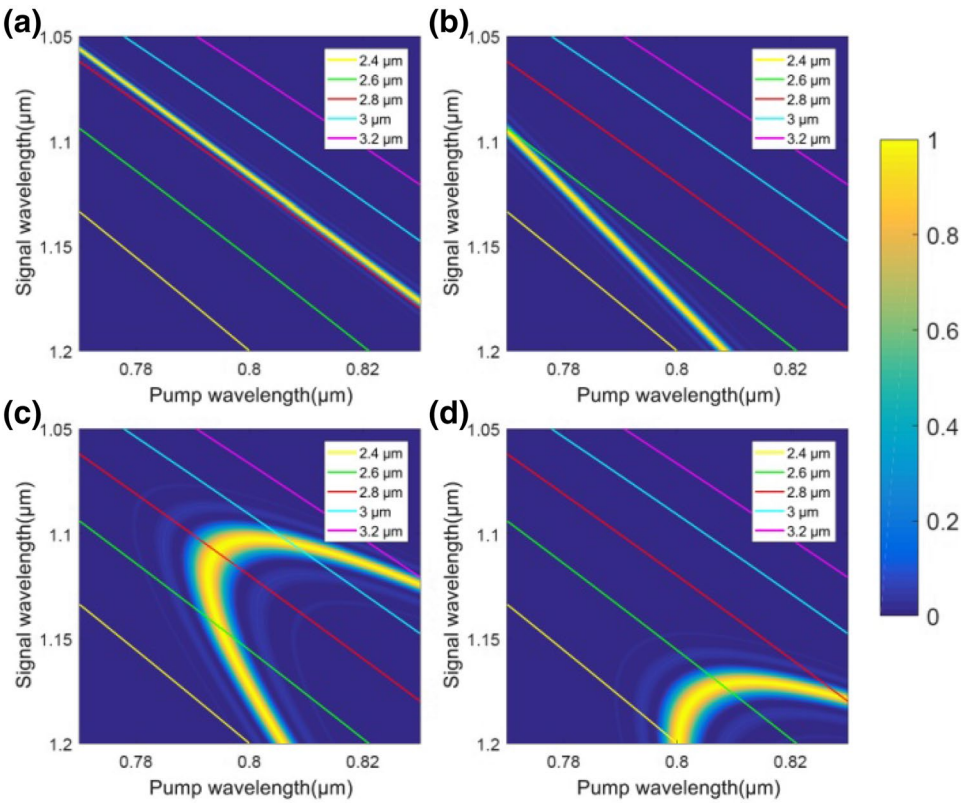

Fig. 2 Phase-matching configurations: **a** collinear configuration, non-collinear configuration with non-collinear angle of **b** 3°, **c** 4°, and **d** 5°. The solid color curves denote the corresponding idler waves. Color bar indicates conversion efficiency under phase-matching condition. As can be seen, with non-collinear angle of 4°, most of the components of the pump spectrum can be utilized and more components of the signal meet high gain to realize broadband amplification

$$\frac{\mathrm{d}E^{\mathrm{idler}}_{\mathrm{eff},q}(\omega_q)}{\mathrm{d}z} = \frac{i\omega_q}{n^q_{\omega_q}(\theta_{\mathrm{idler}})c} d_{\mathrm{eff}} \sum_{o=1}^{N_1}\sum_{p=1}^{N_2} E^{\mathrm{pump}}_{\mathrm{eff},o}(\omega_o)\left[E^{\mathrm{sig}}_{\mathrm{eff},p}(\omega_p)\right]^* e^{i\Delta kz}\delta_{\omega_o,\omega_p+\omega_q}, \tag{3}$$

where $\Delta k = k_o(\theta_{\mathrm{pump}}) - k_p(\theta_{\mathrm{sig}}) - k_q(\theta_{\mathrm{idler}})$, and $\delta_{\omega_o,\omega_p+\omega_q} = \begin{cases} 1, & \omega_o = \omega_p + \omega_q \\ 0, & \omega_o \neq \omega_p + \omega_q \end{cases}$.

Here, E is the electric-field amplitude, d_{eff} is the effective second-order nonlinearity, ω is the angular frequency, n is the refractive index (considering the polarization of the corresponding waves), c is the light speed in vacuum, and k is the wave vector. The subfixes o, p, and q represent different frequency components of pump, signal, and idler wave, respectively. The superscript "asterisk" stands for the complex conjugate. The non-collinear angle $\alpha = \theta_{\mathrm{sig}} - \theta_{\mathrm{pump}}$ is contained in the phase-mismatching term Δk. The details of the theoretical derivation will be presented in a forthcoming publication. Those equations can only be solved by numerical method. By taking Sellmeier equation of the KTA material into Eqs. (1)–(3), the method can be applied to evaluate parametric conversion efficiency and the output spectrum of the signal and idler. With this method, it was found that 4.2° is the optimum non-collinear angle under which the OPA process supports the broadest spectrum output for both signal and idler.

350 μJ of the pump was collimated to 2 mm in diameter by a telescope in the second stage and the signal was amplified to 22 μJ. In the third stage, both the pump and the signal were collimated to 4 mm in diameter and the signal pulse was amplified to 150 μJ with 1-mJ pumping. In the final stage, the pump and the signal were both collimated into the KTA crystal. The diameter of the pump beam was 8 mm and that of signal was slightly larger. By applying 10 mJ of the pump energy, the signal was boosted to 1.8 mJ and the idler we got was 520 μJ, reaching a total conversion efficiency of 23.2%. Increasing the pump energy in the final stage, supercontinuum generation occurred in the KTA crystal; thus, further energy scaling is limited in this stage. Evolution of the signal spectrum in different stages and the spectrum of the idler are shown in Fig. 3a, b, respectively. Pump-to-idler conversion efficiency of 4.7% is calculated by the theoretical method to evaluate the DFG process in the last stage and the calculated spectrum of the idler with nearly 500-nm bandwidth is plotted in red solid curve, as shown in Fig. 3b. As a comparison, the experimental results of pump-to-idler conversion efficiency and idler bandwidth are 5.2% and 525 nm, respectively. The bandwidth corresponds to Fourier-transform-limited (FTL) pulse duration of 27 fs. A slight discrepancy between experiment and simulation

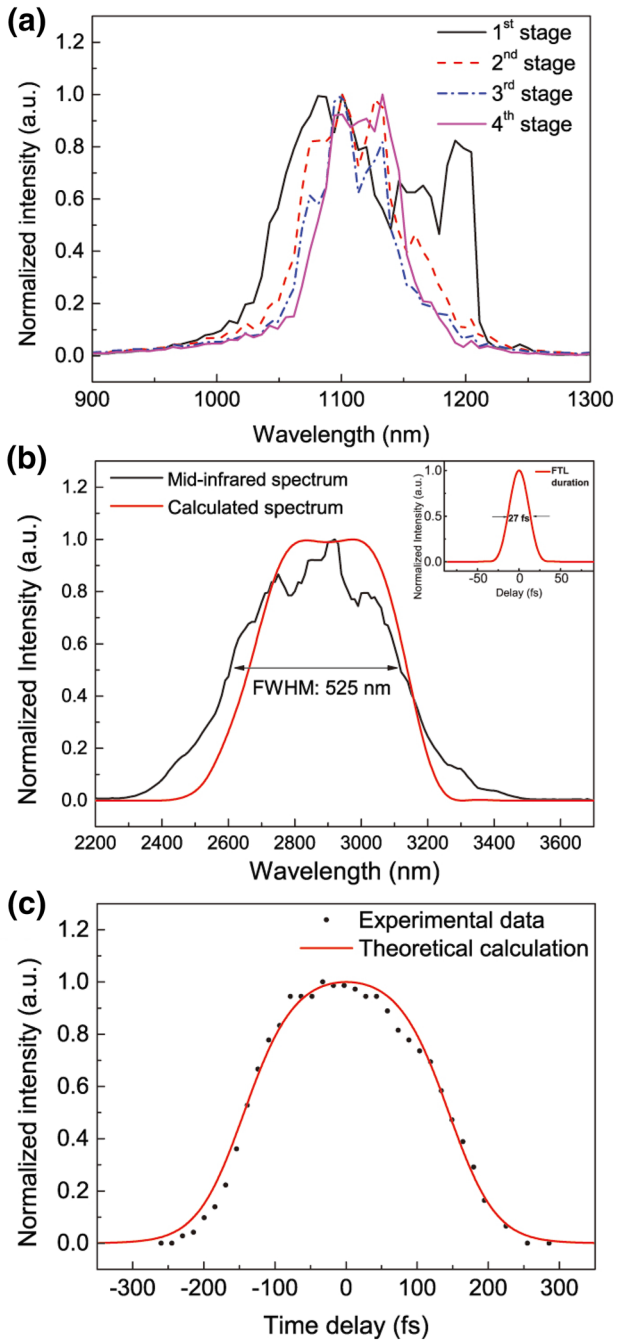

Fig. 3 **a** Evolution of the signal spectrum in different parametric amplification stages; **b** measured and calculated spectra of the output mid-infrared laser (considering the spectrum of pump and signal wave as with a Gaussian profile), inset: the Fourier-transform-limited (FTL) pulse duration of the idler; **c** experimental data of cross-correlation intensity of sum–frequency of the pump and the idler is shown in red dots. Theoretical calculation is shown in blue solid curve, assuming that the pulse duration of the mid-infrared laser is 100 fs

results is due to that Gaussian profile is assumed for signal spectrum in our simulation, whereas the actual profile is not quite so simple. The theoretical method is proved to work well by our experiment and can also be applied to OPCPA system design to evaluate the characteristics of parametric process.

Sum–frequency cross correlation was adopted to characterize the pulse duration of the idler. A small portion of the 40-fs pump laser and the idler were non-collinearly sent into a 0.141-mm BBO crystal with a small angle to separate them from the sum–frequency signal. A delay line was set to adjust the time delay of the pump laser relative to that of the idler. Bright orange sum–frequency signal around 626 nm occurs when the pump and the idler overlap temporally. The intensity of the signal was recorded while adjusting the relative time delay and is plotted in black dots, as shown in Fig. 3c. The theoretical intensity distribution of the sum–frequency signal against the time delay was calculated, assuming that the pulse duration of the idler is 100 fs and is plotted in red solid curve, as shown in Fig. 3c. The theoretical curve meets well with the experimental data which indicates that the pulse duration of the idler is around 100 fs. The measured pulse duration is much longer than the FTL pulse duration and can be explained as below. KTA crystal shows normal dispersion for the signal wave (143.3 fs^2/mm for 1.115 μm); therefore, the signal experiences pulse stretching with redder part of the spectrum travelling on the pulse front. Thus, the generated idler shows down-chirped characteristic during the DFG process. Besides, the idler experiences anomalous dispersion (− 243.8 fs^2/mm for 2.864 μm) when travelling through KTA crystal and thus is stretched to longer pulse. Further compression and characterization for the mid-infrared pulse will be carried out in the future.

In summary, 520-μJ, 1-kHz, broadband mid-infrared femtosecond laser at 2.8 μm is generated. Theoretical method was developed to give an optimum non-collinear angle and estimate the output spectrum and conversion efficiency. As a result, the conversion efficiency (pump to idler) of 5.2% and the output spectral bandwidth of 525 nm are close to that of our numerical calculation, which indicates that our theoretical method is suitable for calculation of parametric process. Further improvement will focus on efficient signal generation and OPCPA to support more energetic pulse generation by increasing pump energy. Yin et al. [19] realized micro-Joule-level octave-spanning mid-infrared signal generation directly from one stage by intra-band DFG, which holds promise for compact high-energy few-cycle mid-infrared pulse generation and thus for shorter attosecond pulse generation due to its passively stable carrier envelop phase [20]. Higher pulse energy may be achieved using the technique of dual-chirped optical parametric amplification to generate more intense ultrashort mid-infrared laser [21, 22]. Such a laser could be a promising candidate for generation of higher order harmonics and supercontinuum white-light laser [23].

Acknowledgements This work was partially supported by the National Key Scientific Instruments Development Program of China (2012YQ120047), the National Natural Science Foundation of China under Grant Nos. 61575217 and 11774410, and the Strategic Priority Research Program of Chinese Academy of Sciences under Grant No. XDB16030200

References

1. P. Colosimo, G. Doumy, C.I. Blaga, J. Wheeler, C. Hauri, F. Catoire, J. Tate, R. Chirla, A.M. March, G.G. Paulus, H.G. Muller, P. Agostini, L.F. DiMauro, Nat Phys. **4**, 386 (2008)
2. B. Shan, Z. Chang, Phys. Rev. A. **65**, 011804 (2001)
3. A.D. Shiner, C. Trallero-Herrero, N. Kajumba, H.C. Bandulet, D. Comtois, F. Légaré, M. Giguère, J.C. Kieffer, P.B. Corkum, D.M. Villeneuve, Phys. Rev. Lett. **103**, 073902 (2009)
4. Y. Deng, A. Schwarz, H. Fattahi, M. Ueffing, X. Gu, M. Ossiander, T. Metzger, V. Pervak, H. Ishizuki, T. Taira, T. Kobayashi, G. Marcus, F. Krausz, R. Kienberger, N. Karpowicz, Opt. Lett. **37**, 4973 (2012)
5. K.-H. Hong, C.-J. Lai, J.P. Siqueira, P. Krogen, J. Moses, C.-L. Chang, G.J. Stein, L.E. Zapata, F.X. Kärtner, Opt. Lett. **39**, 3145 (2014)
6. Y. Yin, J. Li, X. Ren, K. Zhao, Y. Wu, E. Cunningham, Z. Chang, Opt. Lett. **41**, 1142 (2016)
7. S.L. Cousin, F. Silva, S. Teichmann, M. Hemmer, B. Buades, J. Biegert, Opt. Lett. **39**, 5383 (2014)
8. M.C. Chen, P. Arpin, T. Popmintchev, M. Gerrity, B. Zhang, M. Seaberg, D. Popmintchev, M.M. Murnane, H.C. Kapteyn, Phys. Rev. Lett. **105**, 173901 (2010)
9. J. Li, X. Ren, Y. Yin, Y. Cheng, E. Cunningham, Y. Wu, Z. Chang, Appl. Phys. Lett. **108**, 231102 (2016)
10. J. Li, X. Ren, Y. Yin, K. Zhao, A. Chew, Y. Cheng, E. Cunningham, Y. Wang, S. Hu, Y. Wu, Nat. Commun. **8** (2017)
11. G. Andriukaitis, T. Balčiūnas, S. Ališauskas, A. Pugžlys, A. Baltuška, T. Popmintchev, M.-C. Chen, M.M. Murnane, H.C. Kapteyn, Opt. Lett. **36**, 2755 (2011)
12. K. Zhao, H. Zhong, P. Yuan, G. Xie, J. Wang, J. Ma, L. Qian, Opt. Lett. **38**, 2159 (2013)
13. T. Popmintchev, M.-C. Chen, D. Popmintchev, P. Arpin, S. Brown, S. Ališauskas, G. Andriukaitis, T. Balčiunas, O.D. Mücke, A. Pugzlys, Science **336**, 1287 (2012)
14. S. Wandel, G. Xu, Y. Yin, I. Jovanovic, J. Phys. B: At. Mol. Opt. Phys. **47**, 234016 (2014)
15. S. Wandel, M.-W. Lin, Y. Yin, G. Xu, I. Jovanovic, Opt. Express. **24**, 5287 (2016)
16. L. von Grafenstein, M. Bock, D. Ueberschaer, K. Zawilski, P. Schunemann, U. Griebner, T. Elsaesser, Opt. Lett. **42**, 3796 (2017)
17. M. Baudisch, M. Hemmer, H. Pires, J. Biegert, Opt. Lett. **39**, 5802 (2014)
18. Y. Chen, Y. Li, W. Li, X. Guo, Y. Leng, Opt. Commun. **365**, 7 (2016)
19. Y. Yin, X. Ren, A. Chew, J. Li, Y. Wang, F. Zhuang, Y. Wu, Z. Chang, Sci. Reports **7**, 11097 (2017)
20. A. Baltuška, T. Fuji, T. Kobayashi, Phys. Rev. Lett. **88**, 133901 (2002)
21. Q. Zhang, E.J. Takahashi, O.D. Mücke, P. Lu, K. Midorikawa, Opt. Express. **19**, 7190 (2011)
22. Y. Yin, J. Li, X. Ren, Y. Wang, A. Chew, Z. Chang, Opt. Express. **24**, 24989 (2016)
23. B.-Q. Chen, C. Zhang, C.-Y. Hu, R.-J. Liu, Z.-Y. Li, Phys. Rev. Lett. **115**, 083902 (2015)